Electron-phonon scattering rates in complex polar crystals

M. P. Prange,[1,*] L. W. Campbell,[2] and S. Kerisit[1]

[1]*Physical and Computational Sciences Directorate, Pacific Northwest National Laboratory, Richland, Washington 99354, USA*

[2]*National Security Directorate, Pacific Northwest National Laboratory, Richland, Washington 99354,USA*

(Received 17 October 2016; revised manuscript received 6 July 2017; published 18 September 2017)

The thermalization of fast electrons by phonons is studied in CsI, NaI, SrI_2, and $YAlO_3$. This numerical study uses an improvement to a recently developed method based on a density functional perturbation description of the phonon modes that provides a way to go beyond widely used phonon models based on binary crystals. The method is compared to standard *ab initio* approaches to the electron-phonon interaction. Improvements to this method are described, and scattering rates are presented and discussed. The relative activity of the numerous phonon modes in materials with complicated structures is discussed, and a simple criterion for finding the modes that scatter strongly is presented.

DOI: 10.1103/PhysRevB.96.104307

I. INTRODUCTION

Detailed theoretical and experimental investigations over the last decade have shown that the thermalization phase of a scintillation event plays a significant role in determining the ultimate performance of scintillating gamma-ray detectors [1–7]. While much of the underlying physics is now well understood, significant gaps remain regarding the complicated sequence of events following gamma excitation of a polar crystal, in particular, competing effects arising from the different mobilities and lifetimes of the various excitations that are present in scintillating materials. In the course of this discovery, it has been noted that ionic crystals with more than two atoms in a unit cell show less resolution limiting nonproportionality than similar materials with simple crystal structures. It has been hypothesized [8–11] that the improved performance in complex crystals may result from reduced charge separation. As the secondary electrons travel away from the less mobile holes, they are less able to escape to remote regions of the crystal if the crystal structure has low symmetry. These electrons, therefore, are more likely to recombine with holes and ultimately contribute to the optical signal. Analyzing this type of hypothesis requires detailed knowledge of the microscopic physics, including the thermalization distances and times of initially hot electrons created in the energy cascade. This thermalization occurs mainly through interaction with the phonons, which have mostly been treated with phenomenological models that apply best to systems with small, simple unit cells [2,5–7,12]. Detailed evidence on the dynamics of the energy cascade is emerging from modeling and experiment [3,11,13–17], however uncertainty remains about the population of various types of secondary excitations, their dynamics, and mutual interactions. Importantly, the amount of energy and momentum relaxation that is due to optical and acoustic phonons differs widely in various models [6,7,18–20]. A major challenge to understanding the energy cascade is the highly excited nature of the relevant degrees of freedom. In contrast to situations arising from the application of low-energy electromagnetic fields and temperature gradients (e.g., as encountered in the design of electronic devices), the energy cascade involves carriers with kinetic energy comparable to the band gap of the material (i.e., several eV). This implies that carriers are not well described by quasiparticles near band extrema.

In an effort to direct searches for improved scintillators and shed light on these questions, we have recently developed a semiclassical theory [21] to estimate the rate of energy transfer between hot electrons produced in the cascade initiated by the absorption or Compton scattering of a gamma-ray photon. In the present paper we describe refinements to this theory that improve the accuracy and computational feasibility of the method. We provide updated results for CsI, new results for NaI, and new results for two complex polar scintillators: strontium iodide (SrI_2) and yttrium aluminum perovskite (YAP, $YAlO_3$). The first two materials are included because they have been extensively studied and are widely used; they also have simple two-atom cubic unit cells. The other two materials are more complex structurally (with 24 and 20 atoms in their primitive unit cells) and representative of materials considered in the search for improved scintillators. The low-energy carrier transport in SrI_2 is of current interest because SrI_2 is a bright and proportional scintillator [22]. The fundamental reasons for this high performance are still unknown [23,24]. YAP is interesting because it has excellent nonproportionality characteristics [25,26]. Of the two complex materials, SrI_2 has soft phonon modes typical of ionic alkali- and alkaline earth halides while YAP, a representative oxide, exhibits very stiff vibrations. These different phonon properties lead to different scintillation behavior, and a description of both types of materials within a common framework is desirable. This paper joins a growing body of work [27–29] using *ab initio* methods to understand atomic-scale phenomena and their relation to radiation detector performance.

II. COMPUTATIONAL METHODS

In Ref. [21] we formulated a semiclassical theory of the electron-phonon interaction. This theory was derived from a viewpoint complementary to the standard, fully quantum formulation of the electron-phonon interaction [30–35] in which the fundamental quantity is the coupling $g_{\mathbf{k},\mathbf{k}'} = \langle \mathbf{k}'|H_{ep}|\mathbf{k}\rangle$ between electronic quasiparticle states $|\mathbf{k}\rangle$ and $|\mathbf{k}'\rangle$.

*micah.prange@pnnl.gov

The quasiparticles are described as Bloch waves (with band and crystal momentum indices in the composite $\mathbf{k}$) resulting from density functional theory (DFT) calculations, sometimes with quasiparticle effects beyond DFT included (e.g., in the GW framework). H_{ep} is a coupling Hamiltonian that must be specified. The advent of robust implementations of density functional perturbation theory allowed the *ab initio* calculation of both phonon structures and the electron-phonon interaction [36–38]. In this context, H_{ep} is taken as the first-order change in the Kohn-Sham (KS) Hamiltonian in response to deformation of the structure corresponding to excitation of a phonon. This choice is intuitive and theoretically justified by Giustino [39]. This quantum theory of the electron-phonon interaction has been applied to a variety of systems including metals [40], semiconductors [41,42], and even hot carrier thermalization in insulators [43]. These calculations have been found to require dense sampling in reciprocal space; practical access to useful results was greatly improved by the application of Fourier interpolation of the phonon structures and matrix elements to achieve sufficient sampling of the Brillouin zone. Approaches representing the electronic orbitals in terms of maximally localized Wannier functions have made converged results more accessible [42,44–46].

The approach developed here is motivated by a desire to get away from a band-structure description of the quasiparticles. Such descriptions become increasingly complicated as the quasiparticle kinetic energy grows beyond the first band crossing and more bands become accessible. Energy cascades produce quasiparticles of very high energy which decay by a variety of processes. For quasiparticles with kinetic energy similar to and lower than the band gap of the material, the quasiparticle-phonon interaction is the primary relaxation channel. The model of the current paper is targeted at quasiparticle kinetic energies of several eVs in complex systems, a regime where there are many bands throughout the Brillouin zone accessible to the carriers. A quantum description of the quasiparticles is hampered by the large number of bands. When there is only one band available, the direction of the crystal momentum and its magnitude (or, equivalently, the energy) determine the quasiparticle wave function and the physical properties of the quasiparticle. When there are many bands available, eigenstates are in general linear combinations of many Bloch waves. In this case tabulation of the $g_{\mathbf{k},\mathbf{k}'} = \langle \mathbf{k}'|H_{ep}|\mathbf{k}\rangle$ becomes cumbersome, as does application of the matrix elements in mesoscale simulations which require some kind of averaging over the available states or an explicit description of the carrier wave function.

Since significant modeling of energy cascade events has been performed using a classical description of the quasiparticles produced by high-energy (MeV) excitation [2–8,47,48], we have chosen to use the same description in this work. This means the energy and momentum of the quasiparticle follow the classical dispersion $E = k^2/2$, and the carrier's trajectory $\mathbf{r}(t)$ is a succession of constant-velocity ballistic legs interrupted by scatterings from phonons. The rate and distribution of energy transfers of such scatterings are the main quantities sought in this work. To make a useful model that can be applied when only the particle velocity is known, we average over initial positions $\mathbf{r}(0)$ of the trajectories uniformly distributed in the unit cell of the crystal. As in the conventional theory of the electron-phonon interaction, the quantum nature of the phonon structure is kept in the current theory. We use standard density functional perturbation theoretic (DFPT) calculations of the phonons and the first-order induced densities associated with lattice distortions and static homogeneous applied electric fields. Since this approach is different than the conventional one, we will note the relationship between expressions encountered in our semiclassical theory to their counterparts in the conventional, fully quantum one which is described well in Refs. [39,49].

To derive expressions for the scattering rate Γ suffered by our classical point particle, we assume that it interacts with the lattice vibrations of an insulating crystal via a simple screened Coulomb interaction

$$v_{\mathrm{sc}} = 4\pi\left(\frac{\epsilon_\infty^{-1}}{q^2} + \frac{1-\epsilon_\infty^{-1}}{q^2+k_{\mathrm{tf}}^2}\right) \tag{1}$$

that goes to the bare Coulomb interaction $4\pi/q^2$ at large momentum transfers q and to an interaction $4\pi\epsilon_\infty^{-1}/q^2$ screened by the frozen-lattice dielectric constant ϵ_∞ at small q. The crossover wave vector is taken as the Thomas-Fermi wave vector k_{tf} of the homogeneous electron gas with the same average density as the valence electrons in the crystal.

We then treat this interaction as a perturbation to the phonon system. We derive the following golden-rule type expression for the rate of excitation (upper sign) or deexcitation (lower sign) of the $\lambda,\mathbf{q}$ phonon mode by a charged particle traveling through a crystal:

$$\Gamma_{\lambda,\mathbf{q}}^{(\pm)} = \frac{2\pi N}{V}\sum_{\mathbf{G}} |v_{\mathrm{sc}}(\mathbf{q}+\mathbf{G})n_\lambda(\mathbf{q}+\mathbf{G})|^2 \times \delta\left(\pm\omega_{\lambda,\mathbf{q}} - (\mathbf{q}+\mathbf{G})\cdot\mathbf{v} + \frac{1}{2}(\mathbf{q}+\mathbf{G})^2\right). \tag{2}$$

In our notation, λ indexes the phonon branch, $\mathbf{q}$ and $\mathbf{G}$ are momenta from the first Brillouin zone and the reciprocal lattice, respectively, V/N is the volume of the unit cell of the crystal, $\mathbf{v}$ is the velocity of the charged particle that is traversing the material, and $\omega_{\lambda,\mathbf{q}}$ is the phonon energy. We use Hartree atomic units ($e^2 = \hbar = m = 1$).

Equation (2) is based on the electrostatic interaction between two charge distributions: the perturbing charge [taken as a point charge screened by the sample electrons via Eq. (1)] and the density n_λ induced by the excitation of the phonon branch λ. This interaction is then averaged over positions of the perturbing point charge in the crystal.

In the conventional, quantum formulation of the electron-phonon interaction, an expression very similar to Eq. (2) is derived from a different perspective. In this case, the electrons are treated quantum mechanically as well as the phonons. A complete field-theoretic derivation of an expression of the form of Eq. (2) is given by Giustino [39] in Eq. (169). A thorough discussion of the derivation lists all the approximations involved. Inspection shows that this expression is identical to Eq. (2) except that the electron-phonon matrix elements $g_{\mathbf{k},\mathbf{k}'} = \langle \mathbf{k}'|H_{ep}|\mathbf{k}\rangle$ of Ref. [39] are replaced by $v_{\mathrm{sc}}(\mathbf{q}+\mathbf{G})n_\lambda(\mathbf{q}+\mathbf{G})$ here, and the particle energies (which are usually taken as eigenvalues of KS or GW quasiparticles in the quantum theory) are replaced with their free-electron values $E(\mathbf{k}) = k^2/2$. The physical meanings of these terms is

clear: The electron-phonon coupling scatters (quasi)particles from one state to another by the absorption or emission of a phonon.

The semiclassical theory evaluated in this work has as quasiparticles classical point charges that are screened by the dielectric response of the host material in the role played by the computed KS orbitals in *ab initio* approaches. This is a key difference that makes the current theory compatible with existing kinetic Monte Carlo (KMC) descriptions of the energy cascade in scintillators [6,7,48,50,51] which use a classical description of the electrons and holes. Also, fully quantum theories of the electron-phonon interaction contain exchange-correlation contributions to the interaction Hamiltonian which are absent in the theory of this work. While the difference in the representation of the quasiparticles is stark, the semiclassical theory used here is equivalent to one in which free electrons occupy plane-wave orbitals and interact via the effective interaction $\sum_{\mathbf{q},\lambda} v_{\rm sc} n_{\mathbf{q},\lambda}$.

For materials in their ground state there is no thermal population of phonons and only phonon emission [upper sign in Eq. (2)] needs to be considered. At finite temperature the rates of emission and absorption of phonons through the $\lambda,\mathbf{q}$ channel are

$$[N(T,\omega_{\lambda,\mathbf{q}})+1]\Gamma^{(+)}_{\lambda,\mathbf{q}} \quad \text{and} \quad N(T,\omega_{\lambda,\mathbf{q}})\Gamma^{(-)}_{\lambda,\mathbf{q}}, \tag{3}$$

respectively. Here $N(T,E)$ is the normal Bose occupation factor, which is given in terms of the Boltzmann constant k_B by

$$N(T,E) = (e^{E/(k_B T)} - 1)^{-1}. \tag{4}$$

The total rates of phonon emission or absorption are obtained by summing over the various phonon modes:

$$\begin{aligned}\Gamma^{(\pm)} &= \sum_{\lambda,\mathbf{q}} \Gamma^{(\pm)}_{\lambda,\mathbf{q}} = \sum_{\lambda} \int_{\rm BZ} \frac{d\mathbf{q}}{(2\pi)^3} \Gamma^{(\pm)}_{\lambda,\mathbf{q}} \\ &= \frac{8\pi^2 Z^2 N}{V} \sum_{\lambda} \int \frac{d\mathbf{Q}}{(2\pi)^3} |v_{\rm sc}(\mathbf{Q}) n_\lambda(\mathbf{Q})|^2 \\ &\quad \times \delta\left(\pm\omega_{\lambda,\mathbf{q}} - \mathbf{Q}\cdot\mathbf{v} + \frac{Q^2}{2}\right).\end{aligned} \tag{5}$$

The first integral in Eq. (5) is over the Brillouin zone, and the second is extended to all of reciprocal space by the sum over the reciprocal lattice. We use the shorthand that $\mathbf{q}$ is the unique momentum from the first Brillouin zone that differs from $\mathbf{Q}$ by a reciprocal lattice vector. The integrand in Eq. (5) is the probability density for a phonon scattering event that transfers energy $\pm\omega_{\lambda,\mathbf{q}}$ and momentum $\pm\mathbf{Q}$ from the particle to the vibrational modes of the crystal. The energy-conserving δ function in Eq. (5) yields a $2d$ integral over a surface that is a sphere of radius $\sqrt{v^2 \mp 2\omega_{\lambda,\mathbf{q}}}$ centered at $\mathbf{v}$ when $\omega_{\lambda,\mathbf{q}}$ is constant. Averages of the quantity X over the scattering events can be found using similar integrals:

$$\begin{aligned}\langle X^{(\pm)}\rangle &= \frac{8\pi^2 Z^2 N}{\Gamma^{(\pm)} V} \sum_{\lambda} \int \frac{d\mathbf{Q}}{(2\pi)^3} |v_{\rm sc}(\mathbf{Q}) n_\lambda(\mathbf{Q})|^2 X(\mathbf{v},\mathbf{Q}) \\ &\quad \times \delta\left(\pm\omega_{\lambda,\mathbf{q}} - \mathbf{Q}\cdot\mathbf{v} + \frac{Q^2}{2}\right).\end{aligned} \tag{6}$$

Our strategy is to use Eq. (5) to find $\Gamma^{(\pm)}$ and then use Eq. (6) with X being, e.g., the cosine of the scattering angle. The integrals are completed numerically using techniques described in Ref. [21] and below. These results then provide an average picture of the scattering that can be parameterized in simplified microscopic models such as KMC simulations: $\Gamma^{(\pm)}$ determines how often the particles scatter, and $\langle\cos\theta\rangle$ and $\langle\omega_{\lambda,\mathbf{q}}\rangle$ determine how fast the propagation direction and speed, respectively, relax.

In Ref. [21], we calculated n_λ numerically on a grid in reciprocal space within the plane-wave framework of the ABINIT code [36,37,52,53]. Subsequent experience has shown that it is difficult to produce the correct small-q behavior in such calculations. The acoustic modes at the zone center correspond to phonons with vanishing frequency: The crystal is simply translated in space with constant velocity. An electron drifting with such a crystal should not be scattered. Mathematically, this situation corresponds to the small-q limit. This limit is important because the factors of $\mathbf{q}+\mathbf{G}$ in the denominator heavily weight small-q scattering events; the numerator needs to vanish sufficiently fast to ensure that the $\mathbf{q}=\mathbf{0}$ acoustic modes do not introduce unphysical scattering. This is related to the acoustic sum rule [34] as described below.

A. Effective charge approximation

To arrive at a numerical procedure that is stable, tractable, and well-behaved near Γ, we have calculated the induced density in response to atomic displacements from the Born effective charge tensor $Z^*_{\kappa,\beta\alpha}$. This quantity can be equivalently defined as the force on an atom in the κ sublattice under a macroscopic electric field (per unit applied field) or the linear coefficient in an expansion of the macroscopic polarization (in the direction β) per unit cell in response to displacement (in the direction α) of the κ sublattice [34,36]. In this formulation, we take

$$\begin{aligned}n_\lambda(\mathbf{q}+\mathbf{G}) &= \sum_{\kappa,\alpha} \frac{u^*_{\kappa,\alpha,\lambda}(\mathbf{q})}{\sqrt{2M_\kappa\omega_{\lambda,\mathbf{q}}}} \\ &\quad \times \left(-ie^{-i\boldsymbol{\tau}_\kappa\cdot(\mathbf{q}+\mathbf{G})} \sum_{\beta} Z^*_{\kappa,\alpha\beta} \times (\mathbf{q}+\mathbf{G})_\beta\right) \\ &= \sum_{\beta} Z^*_{\lambda,\beta}(\mathbf{q}+\mathbf{G}) \times (\mathbf{q}+\mathbf{G})_\beta.\end{aligned} \tag{7}$$

The phonon vibrations are described by the eigenvectors $u^*_{\kappa,\alpha,\lambda}(\mathbf{q})$ of the dynamical matrix, and $\boldsymbol{\tau}_\kappa$ is the equilibrium position in the central unit cell of the atom belonging to the κ sublattice. For an effective charge tensor proportional to the identity ($Z^*_{\kappa,\alpha\beta} = Z^*_\kappa \delta_{\alpha,\beta}$), the term in parentheses in Eq. (7) reduces to the first-order density response of a point charge Z^*_κ. When we describe a material as polar, we mean it possesses a nonzero $Z^*_{\kappa,\alpha\beta}$.

An advantage of this approach is that the acoustic sum rule can be enforced by adjusting the computed effective charge tensor following Gonze and Lee [36]. This avoids spurious contributions from the acoustic modes near Γ. Acoustic modes

should obey $Z^*_{\lambda,\beta}(\mathbf{q}+\mathbf{G}) \to 0$ as $\mathbf{q} \to \mathbf{0}$ [54]. The effective charge approximation guarantees this is so. Comparison of Eqs. (7) and (2) to Eqs. (S4) and (4) of Ref. [46] shows that the current theory corresponds (up to differences in the descriptions of the electrons) to the long-range part of the electron-phonon vertex in that work. As those authors point out, the long-range part in Ref. [46] away from Γ can be defined in any smooth way that preserves the long-wavelength limit. For example, Vogl [54] defines the short-ranged part of the electron-phonon interactions to be the part that survives if the macroscopic electric field is canceled by an appropriate uniform external field. The long-range part is the remainder. This definition differs from that of Ref. [46] but has the same long-wavelength limit. Both the scattering potential here and the long-range contributions of Verdi *et al.* contribute to scatterings when the macroscopic field vanishes. A more refined theory would include higher order contributions with terms proportional to $(\mathbf{q}+\mathbf{G})_\alpha(\mathbf{q}+\mathbf{G})_\beta$ and higher powers of the momentum. Such a theory would recover the full Hartree response, including all the short-ranged contributions. This neglect is likely to cause our electron-phonon scattering rates to be underestimated.

A further advantage of using the Born effective charges to estimate the density response is that they can be found by considering the response of the energy to a homogeneous electric field [37] instead of collective atomic displacements. This is possible because both responses (to an electric field or to atomic displacements) are related through the dielectric tensor. Since the effective charges are found through the response to a *homogeneous* electric field, within the effective charge approximation the density response can be found with Γ-point calculations for fields in (at most) three directions. Our previous efforts relied on calculations of the induced density on a grid spanning the (irreducible wedge of the) Brillouin zone, leading to the storage of many large density files for fine grids in reciprocal space. Of course the phonon eigenvectors $u^*_{\kappa,\alpha,\lambda}(\mathbf{q})$ still need to be calculated throughout the Brillouin zone, but this can be efficiently accomplished using Fourier interpolation of the dynamical matrices [36], which only need to be directly computed on modest k grids ($8 \times 8 \times 8$ was the largest used in this work). We used $24 \times 24 \times 24$ fine grids for calculation of the phonon structure throughout this work.

Figure 1 shows the effective charge approximation (inferred from an electric-field perturbation at Γ) with direct calculations using atomic-displacement perturbations in CsI. We see that the real and imaginary parts of the induced density (especially at small $\mathbf{Q}$) are well reproduced by the effective charge approximation. The diagonal part of the computed effective charges used in this work are reported in Table I. For the simple systems (CsI, NaI) the effective charge tensor is proportional to the identity matrix by symmetry. Here the acoustic sum rule reduces to one the number of independent degrees of freedom in the calculation of the effective charges. In contrast, the lower symmetry systems (YAP, SrI_2) have different diagonal elements in different directions and nontrivial off-diagonal elements (e.g., the I1 sublattice in SrI_2 moved in the xy plane has a response in the orthogonal in-plane direction of 0.412 elementary charges compared to the diagonal value of −1.24).

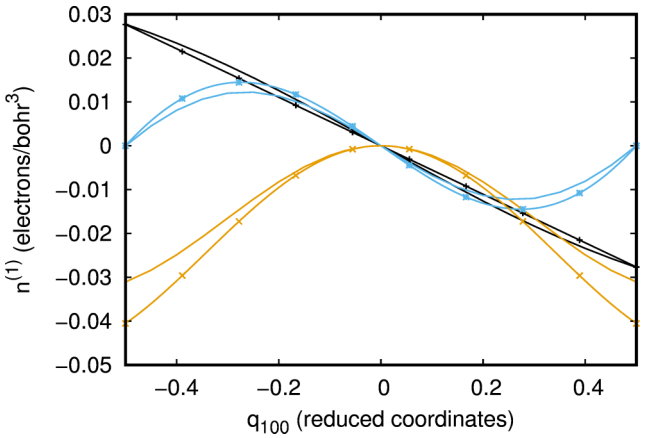

FIG. 1. Computed electronic first-order density response (smooth lines) and the corresponding effective charge approximation (decorated lines) in CsI. The imaginary part of the induced density in response to displacing Cs is in blue (the real part vanishes by symmetry); the real part of the response to I displacements is in yellow; the imaginary part of the I response is in purple.

A drawback of the effective charge approximation described here is that it predicts no induced density (and hence no electron-phonon interaction) in nonpolar materials (e.g., Si where the effective charges vanish by symmetry). In materials with nonvanishing Born effective charge tensors all modes generally contribute, including acoustic modes and optical modes that are transverse at Γ. A further drawback is that the effective charge approximation fails for large wave vectors. The term in parentheses in Eq. (7) (representing the $\mathbf{Q} = \mathbf{q} + \mathbf{G}$ Fourier component of the density response to a 'primitive' perturbation of the κ sublattice in the α direction) is linear in the wave vector $Q = |\mathbf{q}+\mathbf{G}|$ with coefficient $Z^*_{\kappa,\alpha\beta}$ whereas a more realistic model with distributed electron density and a point nucleus will have the same coefficient equal to $Z_\kappa \delta_{\alpha\beta}$ where Z_κ is the atomic number of the atoms occupying sublattice κ. Since $Z^*_{\kappa,\alpha\beta} < Z_\kappa$, the induced density at large wave vector is underestimated in the effective charge approximation. This will reduce the scattering rates of Umklapp processes in our results. An investigation of the magnitude of this effect utilizing the all-electron density and its response to atomic displacements is envisioned for the future.

TABLE I. Diagonal elements of the Born effective charge tensor.

Material	Sublattice	$Z^*_{\alpha\alpha}$	$Z^*_{\beta\beta}$	$Z^*_{\gamma\gamma}$
CsI	Cs	1.32	1.32	1.32
	I	−1.32	−1.32	−1.32
NaI	Na	1.16	1.16	1.16
	I	−1.16	−1.16	−1.16
SrI_2	Sr	2.56	2.70	2.56
	I1	−1.47	−1.24	−1.23
	I2	−1.09	−1.45	−1.32
YAP	O1	−2.28	−2.35	−2.15
	O2	−2.38	−2.13	−2.31
	Y	4.00	3.87	3.70
	Al	2.93	2.96	2.95

B. Adaptive integration

The adaptive integration method used here was described in Ref. [21]. The method is based on partitioning a bounded volume of reciprocal space into cubes in reduced coordinates (corresponding to parallelepipeds in Cartesian coordinates) which are iteratively subdivided into smaller cubes. This subdivision process continues until all contributions to the integral in Eq. (2) are found to sufficient accuracy. In the course of this integration, cubes that do not intersect the surface defined by

$$\pm\omega_{\lambda,\mathbf{q}} - (\mathbf{q}+\mathbf{G})\cdot\mathbf{v} + \tfrac{1}{2}(\mathbf{q}+\mathbf{G})^2 = 0 \qquad (8)$$

are discarded from the list since they do not contribute to the integral. We previously discarded cubes if the left-hand side of Eq. (8) had the same sign at all eight vertices, implying that all of the vertices are either inside (negative sign) or outside (positive sign) the kinematically-allowed surface. This procedure can underestimate the integral by dropping cubes whose vertices all take the same sign but still intersect the kinematically-allowed surface (e.g., if the intersection is confined to one face of the cube). To avoid this kind of error, we have introduced bounding spheres in reciprocal space obtained by setting the phonon frequency in Eq. (8) to 0 (giving a sphere interior to the actual surface) or to the maximum phonon frequency in the material (giving a sphere exterior to the actual surface). The convexity of the parallelepipeds and the spheres implies that any parallelepiped that has all vertices strictly inside the interior sphere does not intersect the interior sphere or the actual surface. Hence any such cubes are dropped from our integration scheme. The bigger problem occurs for parallelepipeds with all vertices exterior. For this case we test for a pair of parallel faces of the parallelepiped that define two planes that do not intersect the exterior sphere. This criterion will always find intersections with the exterior sphere for parallelepipeds whose side length is less than the diameter of the exterior sphere. In practice we have found it to be an effective culling criterion.

Our adaptive integration method has been tested by reproducing analytic results and generally works well. It does, however, leave some very sharp dips and peaks (visible in Figs. 6–9, 11, and 12) that are due to using a finite, constant stopping criterion.

C. Approximations of the current work compared to conventional *ab initio* approaches

Conventional *ab initio* approaches to electron-phonon interactions are based on matrix elements $g_{\mathbf{k},\mathbf{k}'}$ between Bloch Kohn-Sham states $|\mathbf{k}\rangle$ of the first-order change to the Kohn-Sham Hamiltonian induced by phonon excitation [39]. The theory evaluated here differs in the following ways.

(1) The electrons that are scattered are classical particles whose energy is $k^2/2$.

(2) The interaction Hamiltonian is based on the induced Hartree potential and thus neglects exchange-correlation contributions.

(3) The induced Hartree potential itself is calculated according to the effective charge approximation and hence neglects some short-ranged contributions, including the entire electron-phonon interaction for nonpolar materials.

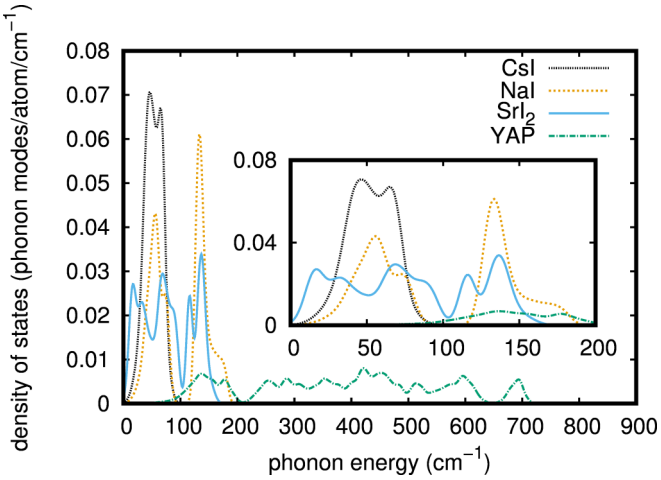

FIG. 2. Computed phonon density of states.

III. RESULTS AND DISCUSSION

This paper includes calculations of four polar scintillating crystals. Two of these are simple (binary) alkali halide systems, and two are more complicated systems of lower symmetry. This selection of materials allows us to make detailed comparisons to existing models (which are only available for small, high-symmetry materials) and explore the effects of lowering symmetry on the electron-phonon interaction. The energy distribution of the phonon modes in the materials studied in the current work is shown in Fig. 2. Experimental data are available for momentum-resolved phonon band structures of CsI [57] and NaI [55,56]. These are compared with theoretical predictions in Ref. [21] (CsI) and Fig. 3 (NaI). We find good agreement with the measured phonon frequencies in these two systems giving us confidence that our numerical approach is accurately capturing the phonon physics. The computed phonon band structures for YAP (Fig. 4) and SrI_2 (Fig. 5) are also shown.

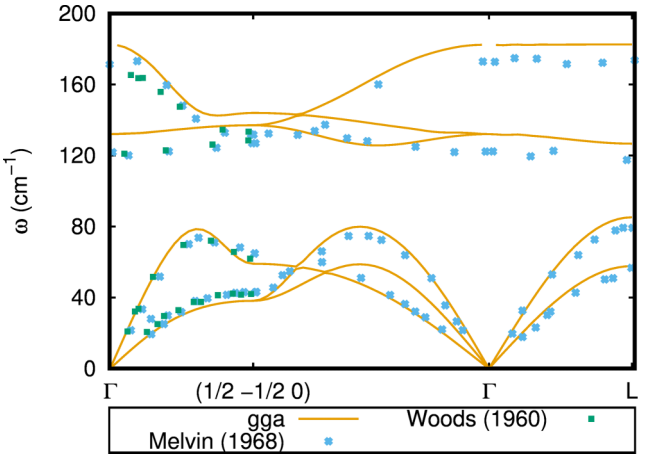

FIG. 3. Computed phonon band structure (in cm^{-1}) along high-symmetry directions in NaI compared to the experimental data of Melvin [55] (+'s) and Woods [56] (x's).

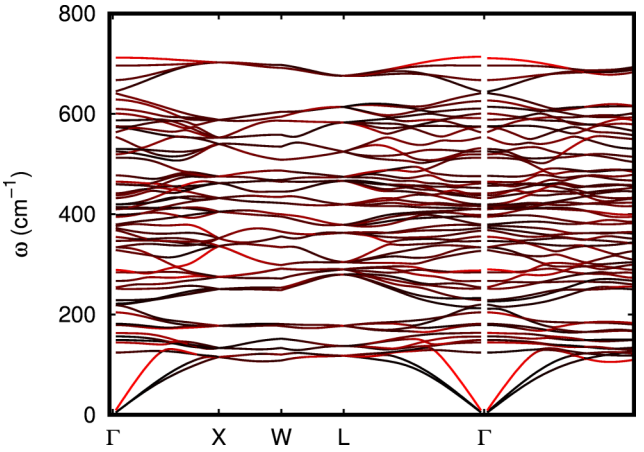

FIG. 4. Phonon band structure (in cm^{-1}) along high-symmetry directions in YAP. The color of the lines indicates the degree to which the mode is longitudinal: Red corresponds to longitudinal modes and black to purely transverse modes.

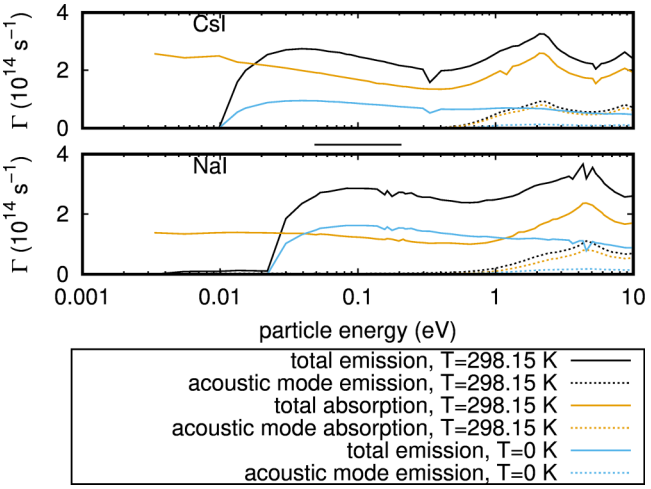

FIG. 6. Total phonon scattering rates in CsI and NaI and the contribution of the acoustic modes at zero and room temperature.

A. Simple alkali halides: CsI and NaI

In our CsI calculations, Troullier-Martins [58] type pseudopotentials obtained from the ABINIT website were used. The Teter parametrization [59] of the local density approximation was employed to calculate the exchange-correlation energy. An $8 \times 8 \times 8\,k$ grid was used resulting in 35 symmetry-inequivalent k points. Good results can be obtained with substantially fewer k points. The NaI system was treated with PBE [60]. Norm-conserving pseudopotentials [61] and a 20 Ha energy cutoff were employed.

Our previous work [21] found that the acoustic modes in CsI contributed significantly to the energy relaxation of fast particles. Through subsequent analysis of those results we have attributed the strong acoustic mode scattering to the failure of the numerical calculations to obey the acoustic sum rule discussed in Sec. II A. Our updated results for scattering rate are shown in Fig. 6, which shows the rates of phonon emission and absorption at two temperatures as a function of particle energy. In these improved calculations, the acoustic modes contribute hardly at all at low energies and only moderately at higher energies. As can be seen in Fig. 6, the acoustic modes contribute at most around 15% of the total scattering at relevant energies at $T = 0$. At higher temperatures, stimulated processes involving acoustic modes become more important since the Bose occupation factors for these low-energy modes turn on at lower temperatures. A similar situation is found in NaI. For these systems, the scattering is dominated by the single longitudinal-optical (LO) phonon mode. At low temperature, the electron-phonon coupling is stronger in NaI than CsI, but the softer longitudinal optical phonon in CsI acquires appreciable thermal population at lower temperature, and stimulated emission and absorption are more important in CsI. Hence, at room temperature, CsI and NaI have similar phonon emission rates.

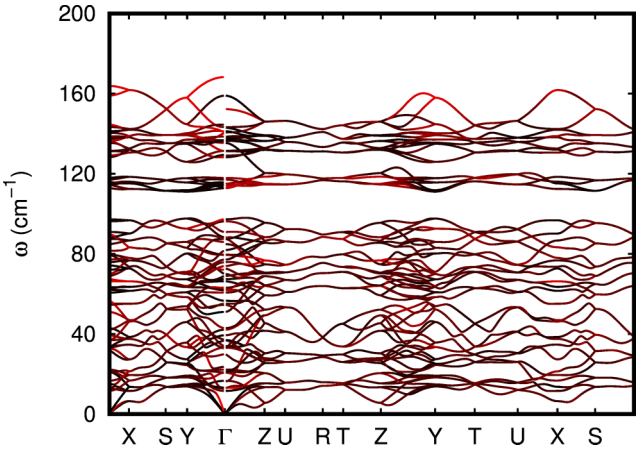

FIG. 5. Phonon band structure (in cm^{-1}) along high-symmetry directions in SrI_2. The color of the lines indicates the degree to which the mode is longitudinal: Red corresponds to longitudinal modes and black to purely transverse modes.

1. *Optical modes in NaI and CsI*

As pointed out above, most of the scattering in the current results involves the long-wavelength LO modes. Although the Fröhlich problem has been considered solved since the 1950's, authoritative, quantitative predictions are not available for hot particles in real systems. A fundamental problem is that the effective mass approximation relating quasiparticle energy and momentum, implicit in the Fröhlich Hamiltonian, is only valid for low-energy particles. Hence, to apply this model, one must choose an effective mass or, at least, some dispersion relation. The dependence of the phonon scattering rate on the quasiparticle dispersion arises from the conservation of energy and momentum: Different phonon processes are allowed for different dispersion relations.

In previous work, we have tried the bare electron mass $m^* = 1$ [7], including the real part of the polaron self-energy in the Fröhlich model itself [6], and using predictions derived from DFT band structures [51]. We compare a Fröhlich model with $m^* = 1$ (as assumed in the current work) and the dielectric constants ϵ_0 and ϵ_∞ from our calculations in Fig. 7. Our calculated dielectric constants are compared to experimental values in Table II. We point out that the current work assumes

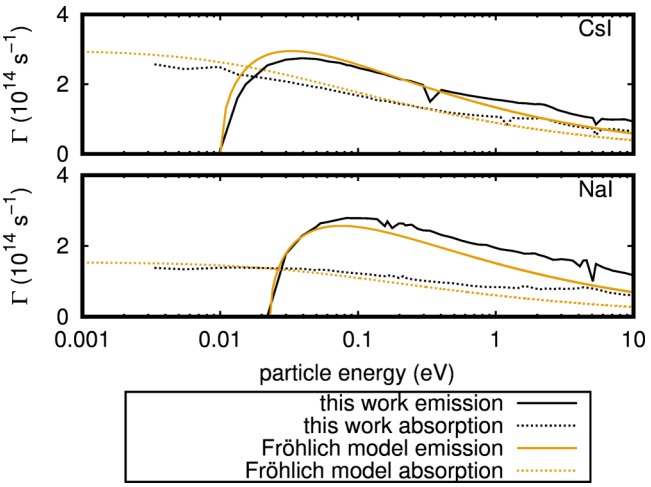

FIG. 7. Scattering rates from the single LO mode in CsI and NaI at room temperature from the current work and the usual phenomenological model evaluated at parameters from our DFT calculations (i.e., $m^* = 1$ and ϵ_0, ϵ_∞ listed in Table II).

$m^* = 1$ in Eq. (2), although other dispersion relations could be implemented in a straightforward way.

2. *Scattering from acoustic and transverse modes in NaI and CsI*

The exchange of energy and momentum between hot electrons and acoustic phonons has been a major challenge limiting simulations of electron transport up to the present. Sparks *et al.* [20] developed the first detailed models of acoustic phonon scattering for hot electron transport that included Umklapp processes. This model was based on the work of Holway and Fradin [63] who used the deformation potential approximation. Holway and Fradin found scattering rates that decreased with increasing particle energy; Sparks and later work by Fischetti *et al.*, [64] on the other hand, found that the inclusion of Umklapp processes gave scattering rates that were much larger at high energies and increased rapidly (like $E^{3/2}$) at high energy. As the experimental picture of hot electron transport in SiO_2 became more established, Bradford and Woolf [62] noted that the high energy behavior of the scattering from acoustic modes in the Sparks and Fischetti models was unphysical. They proposed a model based on a pseudopotential that added a screening term that suppressed Umklapp events and yielded smaller scattering rates. Although originally derived for modeling avalanche breakdown in solids (principally SiO_2), this model and closely related ones have been used for Monte Carlo modeling of scintillator performance in our group [6,7,51] and others [2,8–11]. All these models of acoustic mode scattering are based on the deformation potential approximation which is derived by considering perturbations to the band structure by acoustic vibrations and the subsequent effects on low-energy electrons in a parabolic band. These conditions are not representative of high-energy electrons. To arrive at integrals that can be evaluated analytically for high-energy particles, the above authors were forced to make *ad hoc* and unsatisfying assumptions about the electron-phonon Hamiltonian. In particular, only a single longitudinal acoustic (LA) mode was considered. This is because, for binary systems, the six long-wavelength vibrations are split into four transverse modes (i.e., the dot product of the phonon eigenvectors and $\mathbf{q}$ vanishes as $\mathbf{q} \to \mathbf{0}$) and two completely longitudinal ones: LO and LA branches. Since, in acoustic vibrations, the atoms move sympathetically, the electron-phonon coupling $\epsilon_\infty^{-1} n_\lambda(\mathbf{Q})(4\pi/\mathbf{Q}^2)$ is nonsingular at the origin, and the scattering-rate integral Eq. (5) gets the largest contributions away from Γ. This is why Umklapp processes are important for the acoustic modes. In contrast, for LO phonons, the coupling is singular near Γ, and Fröhlich type scattering is dominated by long-wavelength contributions. The classification into longitudinal and transverse modes cannot be made away from Γ where the modes have mixed character. Since the longitudinal part of the induced density interacts with the longitudinal field of the thermalizing particle, all modes (not just the LA mode) contribute to this type of scattering.

The strategy employed here is complementary to these efforts. We do not use any separate approximations for transverse and acoustic modes: All phonons are treated identically. Instead of relying on models based on zone-center quantities like the speed of sound, we explicitly calculate the phonon eigenvectors. This work is based on detailed calculations of the phonon properties throughout the Brillouin zone. Hence our approach can provide additional information on the nature of the thermalization of hot electrons. Of course the current work also employs approximations. The most severe one for acoustic phonons is probably the effective charge approximation of Eq. (7). Another major approximation is the dispersion relation implicit in the energy-conserving δ function in Eq. (2). However we believe the current work is an improvement on the deformation potential based approximations, is suitable for semiquantitative predictions, and amenable to systematic improvement.

Our results for CsI and NaI are displayed in Fig. 8 which also includes phenomenological models similar to those used in Refs. [6,7] appropriate for these materials. Both of these models use $m^* = 1$ as we have assumed in this work. One of these models includes the screening correction of Bradford and Woolf using a value of $\alpha = 24.3\ \mathrm{nm}^{-1}$ calculated for CsI by Boutboul *et al.* [65]. The main conclusion from this comparison is that the scattering from non-LO modes for high energy (above 3 eV, e.g.) is predicted to be weaker in our semiclassical calculations compared to the Sparks model and shows behavior comparable to the Bradford and Woolf model. The increasingly large scattering rates at high energy that Bradford and Woolf worked to tame are absent in our numerical results, which tend to nearly constant values at high

TABLE II. Computed and experimental [18] dielectric constants. The theoretical numbers were used in the phenomenological model plotted in Fig. 7.

	NaI		CsI	
	Theory	Expt.	Theory	Expt.
ϵ_0	6.63	7.3	6.99	5.65
ϵ_∞	3.47	2.9	3.65	3.0
$1/\epsilon_\infty - 1/\epsilon_0$	0.14	0.21	0.13	0.16

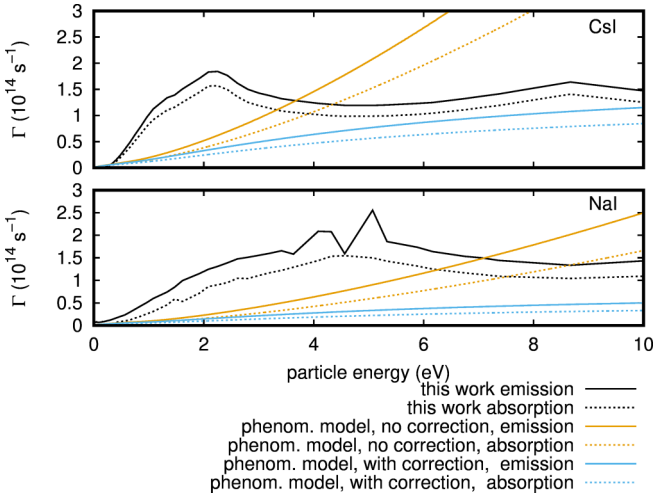

FIG. 8. Scattering rates from the acoustic and transverse optical modes in CsI and NaI at room temperature. The current semiclassical results are compared to phenomenological models following the work of Sparks [20] and Llacer and Garwin [19]. Models are shown with and without the correction proposed by Bradford and Woolf [62].

energies. For low electron energies, our numerical simulations show more electron scattering than any of the deformation potential-based models. We stress that our semiclassical method requires only the atomic structure for input and treats all phonon modes identically.

3. *Average scattering angle*

Besides the scattering rate, information about the momentum relaxation is needed for KMC simulations. For LO modes, predictions can be made from the Fröhlich model [19] about the scattering angle. For other modes, the final momentum of the particle is typically taken in a random direction (or, equivalently, the motion is treated as diffusion with diffusion constant $D = v^2/(3\Gamma)$ where v is the particle speed) [5]. We are interested in how these approximations compare to numerical results in the theory presented here. To this end we show (in Fig. 9) the average cosine of the scattering

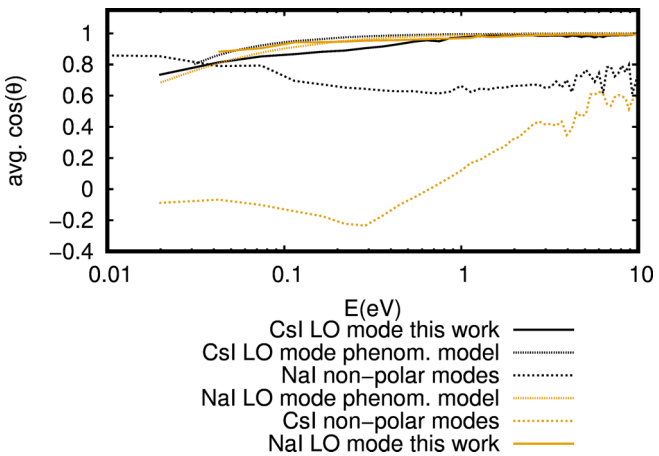

FIG. 9. Average cosine of the scattering angle as a function of particle energy. Results from the phenomenological model for the LO modes of Ref. [51] are also shown.

angle for scattering at $T = 0$ K in NaI and CsI computed via Eq. (6). Also shown are the Fröhlich model results. For the common approximation of a uniformly distributed random direction after scattering the average cosine vanishes. As for the scattering rates, the numerical results are in better agreement with the phenomenological ones for LO modes. At low energies, electrons are seen to mostly backscatter ($\langle\cos(\theta)\rangle < 0$) in CsI while in NaI the scattering is mostly forward. In these calculations, however, the scattering rate for acoustic phonons is small and serves as the denominator in Eq. (6). Hence these results should be viewed skeptically. At higher energies (where non-LO modes are more relevant) our method does not suffer from this problem and predicts scattering that is significantly biased in the forward direction.

B. Complex polar crystals: YAP and SrI_2

Our YAP calculations are based on the structure reported by Ross *et al.* [66]. An energy cutoff of 30 Ha was used; the Brillouin zone was sampled with a $4 \times 4 \times 4$ grid (resulting in 27 k points). As for NaI, the PBE [60] exchange-correlation functional and norm-conserving pseudopotentials [61] were employed. As mentioned above, ABINIT was used for all DFT calculations. Our calculations of SrI_2 are based on the structure reported by Barnighausen and Schulz [67] as obtained from the Crystallography Open Database [68]. Approximations similar to those used for YAP were employed in our calculations for SrI_2. Troullier-Martins type pseudopotentials obtained from the ABINIT website were used. The Teter parametrization [59] of the local density approximation was employed to calculate the exchange-correlation energy. The energy cutoff was set to 10 Ha, and a $8 \times 4 \times 4$ grid of k points was used. Responses to all 72 atomic displacements were considered over the 68 symmetry-inequivalent k points; homogeneous (Γ-point) electric fields in all three directions were also calculated to find the LO-TO splitting in all three directions.

The resulting phonon band structures (Figs. 4 and 5) comprise a rich set of excitations available to the material and lead to multiple pathways for energy and momentum transfer between thermalizing particles and these materials. Full numerical calculations of the scattering rates as a function of the energy of the scattering particle were calculated using the methods described in Sec. II for velocities with no component in the x direction and a y component twice the z component. The total scattering rates for all four materials at $T = 0$ are plotted in Fig. 10.

As expected from its large phonon frequencies, YAP has high scattering rates (several times as large) compared to the other materials considered here. The phonon scattering in YAP along our line of velocities is dominated by a few active modes: mostly by the stiffest LO mode (at an energy of 0.089 eV) with significant contributions from two other optical modes (52 and 20) at 0.089 and 0.073 eV, respectively. The total scattering rate and the contributions from these active modes are exhibited in Fig. 11. In SrI_2, we find the strongest scattering (at zero temperature) from the two stiffest modes and from mode 12. At Γ, these modes have energies of 0.00364, 0.0197, and 0.0208 eV. We show the total scattering rate in SrI_2 and the

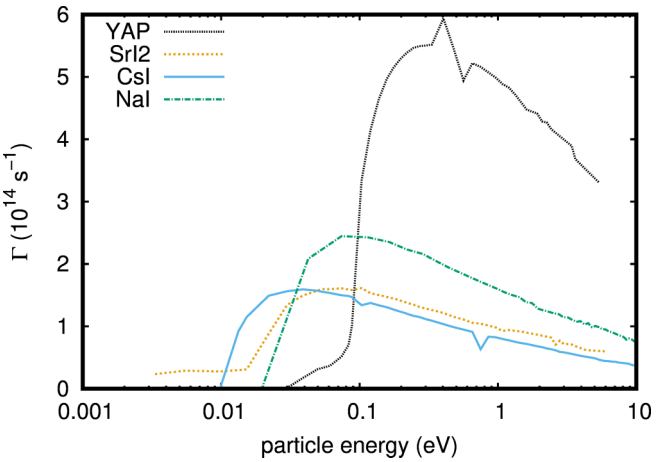

FIG. 10. Total phonon emission rate in inverse seconds at $T = 0$ in a suite of polar crystals.

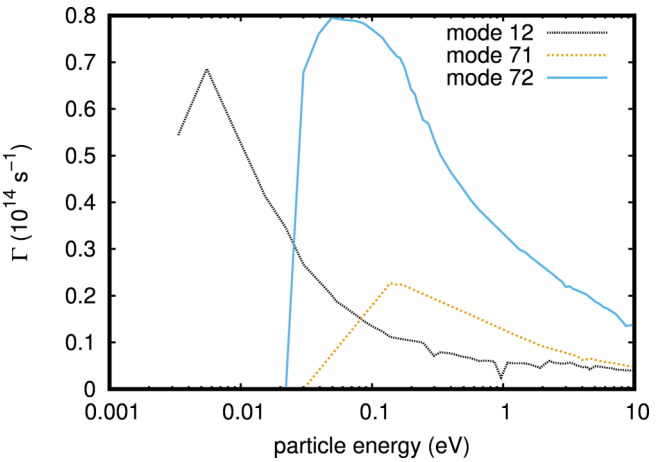

FIG. 12. Contributions to the phonon scattering rate by the three strongest modes in SrI_2 as a function of the energy of the thermalizing particle for particles moving in the yz plane with a y component of the velocity twice the z component.

contributions from these three modes in Fig. 12. Also shown in that plot is the sum of the scattering rates from the three dominant modes. The remainder of the scattering is distributed broadly among the remaining 69 modes: Some modes are not active at all while others contribute small amounts.

In order to understand the relative magnitude of optical modes to scattering, we define a mode-effective charge for velocities along the three Cartesian directions by considering Eq. (7) as $\mathbf{q}$ approaches Γ along the α axis:

$$Z_{\lambda,\alpha} = \sum_{\kappa,\beta} \frac{Z^*_{\kappa,\beta\alpha}}{\sqrt{2M_\kappa}} \lim_{\mathbf{q}\to\mathbf{0}} \frac{u^*_{\kappa,\beta,\lambda}}{\sqrt{\omega_{\lambda,\mathbf{q}}}}. \tag{9}$$

Here the limit is meant to be taken in the α direction. For many optical modes, the scattering rate integral Eq. (5) is dominated by contributions from near the intersection of the kinematically-allowed surface and the line segment connecting the origin and the particle velocity in momentum space. Hence this quantity gives an indication of which modes interact strongly with particles traveling in the α direction. For both

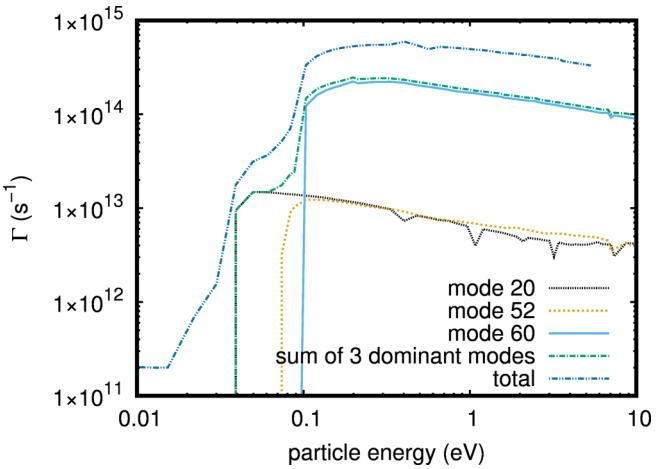

FIG. 11. Contributions to the phonon scattering rate by the three strongest modes in YAP as a function of the energy of the thermalizing particle.

cubic alkali halide systems considered above, $Z_{\lambda,\alpha}$ vanishes for all but the LO mode. This quantity can also be computed from standard phonon calculations of the zone-center properties (i.e., the LO-TO splitting and associated eigenvectors for macroscopic polarization along the three different directions). Hence it is computationally cheap compared to the full Brillouin zone adaptive integration used in our full results. We find the dominant modes listed above among those with large $Z_{\lambda,\alpha}$. Of interest is the fact that a large $Z_{\lambda,\alpha}$ is not sufficient to ensure strong scattering. For example, $Z_{\lambda=69,\alpha=z}$ is 26% of the largest mode effective charge ($Z_{\lambda=72,\alpha=y}$), and, based on this fact, one would expect significant scattering in these calculations. But we find mode 69 makes a very small contribution to the total scattering rate. This implies that a model based on zone-center quantities like $Z_{\lambda,\alpha}$ is insufficient to describe the scattering because it misses the $\mathbf{q}$ dependence of the phonon physics. This observation also points to the need to use fine grids for the phonon quantities to capture the rapid variations of the phonon eigenvectors. We propose that Eq. (9) provides a good screening criteria for strong optical modes in complex systems that could be used to improve the efficiency of full calculations by avoiding large calculations of modes with small effective charges.

In systems with simple phonon structures, all of the low-energy scattering is from the LO mode. Thus, particles whose energy is below the LO phonon energy do not have sufficient energy to emit phonons leading to long thermalization times and lengths when the thermal energy is much smaller than the LO phonon energy. In more complex materials this is no longer the case, and low-energy particles continue to have active energy loss channels. At finite temperature, the situation is more complicated still since a thermalizing particle can successively absorb and emit vibrational quanta from different modes, transferring the energy difference between the two modes to the lattice in the process. Vasilev and co-workers [2,5] have considered this situation and proposed that such sequential scatterings will be more effective at thermalizing particles if the ratio of the greater energy to the smaller one is

less than 2. Based on this criterion, we expect the two stiffest modes in SrI_2 to provide a means for efficient cooling down to low energies.

IV. CONCLUSIONS

We have improved our semiclassical theory of the electron-phonon scattering rates for hot electrons by the implementation of a smooth approximation for the first order density response based on Born effective charges. This advance has permitted the use of fine grids in reciprocal space and made feasible the calculation of large systems of current research interest. We have improved previous work in this area by imposing the acoustic sum rule on the scattering behavior. We have investigated the scattering of electrons by phonons in four important inorganic scintillating crystals by making direct numerical simulations of the phonon scattering rates. These calculations are summarized in Fig. 10. We conclude, in contradiction to our earlier work and long-used phenomenological models based on the deformation potential, that acoustic modes are not the dominant channel for energy relaxation for any energy in polar materials. They are dominated either by scattering from optical phonons or electronic processes. Our method gives a way to calculate the strength of scattering in any polar crystal, and we suggest a numerically cheap way to find the most important thermalizing modes in a given material.

ACKNOWLEDGMENTS

This research was supported by the National Nuclear Security Administration, Office of Defense Nuclear Nonproliferation Research and Development (DNN R&D), of the US Department of Energy (DOE). A portion of the research was performed using PNNL Institutional Computing at Pacific Northwest National Laboratory (PNNL). PNNL is a multi-program national laboratory operated by Battelle Memorial Institute for the US DOE under contract DE-AC0576RL01830.

[1] J. Q. Grim, K. B. Ucer, A. Burger, P. Bhattacharya, E. Tupitsyn, E. Rowe, V. M. Buliga, L. Trefilova, A. Gektin, G. A. Bizarri *et al.*, Phys. Rev. B **87**, 125117 (2013).
[2] R. Kirkin, V. V. Mikhailin, and A. N. Vasil'ev, IEEE Trans. Nucl. Sci. **59**, 2057 (2012).
[3] X. Lu, Q. Li, G. A. Bizarri, K. Yang, M. R. Mayhugh, P. R. Menge, and R. T. Williams, Phys. Rev. B **92**, 115207 (2015).
[4] K. B. Ucer, G. Bizarri, A. Burger, A. Gektin, L. Trefilova, and R. T. Williams, Phys. Rev. B **89**, 165112 (2014).
[5] A. N. Vasil'ev and A. V. Gektin, IEEE Trans. Nucl. Sci. **61**, 235 (2014).
[6] Z. Wang, Y. Xie, L. W. Campbell, F. Gao, and S. Kerisit, J. Appl. Phys. **112**, 014906 (2012).
[7] Z. Wang, Y. Xie, B. D. Cannon, L. W. Campbell, F. Gao, and S. Kerisit, J. Appl. Phys. **110**, 064903 (2011).
[8] H. Huang, Q. Li, X. Lu, Y. Qian, Y. Wu, and R. T. Williams, physica status solidi (RRL) – Rapid Research Letters **10**, 762 (2016).
[9] J. Q. Grim, Q. Li, K. Ucer, R. Williams, G. Bizarri, and W. Moses, MRS Commun. **2**, 139 (2012).
[10] Q. Li, J. Q. Grim, K. B. Ucer, A. Burger, G. A. Bizarri, W. W. Moses, and R. T. Williams, Phys. Status Solidi RRL **6**, 346 (2012).
[11] Q. Li, J. Q. Grim, R. T. Williams, G. A. Bizarri, and W. W. Moses, J. Appl. Phys. **109**, 123716 (2011).
[12] A. Kozorezov, J. K. Wigmore, and A. Owens, J. Appl. Phys. **112**, 053709 (2012).
[13] J. Grim, Q. Li, K. Ucer, A. Burger, G. Bizarri, W. Moses, and R. Williams, Phys. Status Solidi A **209**, 2421 (2012).
[14] G. Bizarri, N. Cherepy, W. Choong, G. Hull, W. Moses, S. Payne, J. Singh, J. Valentine, A. Vasilev, and R. Williams, IEEE Trans. Nucl. Sci. **56**, 2313 (2009).
[15] G. Bizarri, W. Moses, J. Singh, A. Vasil'Ev, and R. Williams, J. Appl. Phys. **105**, 044507 (2009).
[16] G. Bizarri and P. Dorenbos, Phys. Rev. B **75**, 184302 (2007).
[17] G. Bizarri and P. Dorenbos, Phys. Status Solidi C **3**, 3434 (2006).
[18] A. Akkerman, T. Boutboul, A. Breskin, R. Chechik, and A. Gibrekhterman, J. Appl. Phys. **76**, 4656 (1994).
[19] J. Llacer and E. L. Garwin, J. Appl. Phys. **40**, 2766 (1969).
[20] M. Sparks, D. L. Mills, R. Warren, T. Holstein, A. A. Maradudin, L. J. Sham, E. Loh, and D. F. King, Phys. Rev. B **24**, 3519 (1981).
[21] M. P. Prange, L. W. Campbell, D. Wu, F. Gao, and S. Kerisit, Phys. Rev. B **91**, 104305 (2015).
[22] N. J. Cherepy, G. Hull, A. D. Drobshoff, S. A. Payne, E. van Loef, C. M. Wilson, K. S. Shah, U. N. Roy, A. Burger, L. A. Boatner *et al.*, Appl. Phys. Lett. **92**, 083508 (2008).
[23] F. Zhou, B. Sadigh, P. Erhart, and D. Åberg, Npj Comput. Mater. **2**, 16022 (2016).
[24] Q. Li, R. T. Williams, and D. Åberg, Phys. Status Solidi (b) **250**, 233 (2013).
[25] S. B. Donnald, M. Tyagi, H. E. Rothfuss, J. P. Hayward, M. Koschan, M. Zhuravleva, F. Meng, and C. L. Melcher, IEEE Trans. Nucl. Sci. **61**, 332 (2014).
[26] W. Mengesha, T. D. Taulbee, B. D. Rooney, and J. D. Valentine, IEEE Trans. Nucl. Sci. **45**, 456 (1998).
[27] A. Canning, A. Chaudhry, R. Boutchko, and N. Grønbech-Jensen, Phys. Rev. B **83**, 125115 (2011).
[28] A. Chaudhry, R. Boutchko, S. Chourou, G. Zhang, N. Grønbech-Jensen, and A. Canning, Phys. Rev. B **89**, 155105 (2014).
[29] P. Erhart, A. Schleife, B. Sadigh, and D. Åberg, Phys. Rev. B **89**, 075132 (2014).
[30] M. Born and K. Huang, *Dynamical Theory of Crystal Lattices*, Oxford Classic Texts in the Physical Sciences (Oxford University Press, Oxford, UK, 1998).
[31] J. M. Ziman, *Electrons and Phonons: The Theory of Transport Phenomena in Solids*, The International Series of Monographs on Physics (Clarendon Press, Oxford, 1996).
[32] D. Pines, *Elementary Excitations In Solids*, Advanced Book Classics (Westview Press, Boulder, 1999).
[33] G. D. Mahan, *Many-Particle Physics*, Physics of Solids and Liquids (Springer, New Delhi, 2000).

[34] R. M. Pick, M. H. Cohen, and R. M. Martin, Phys. Rev. B **1**, 910 (1970).
[35] H. Frohlich, Proc. R. Soc. Lond. A Math. Phys. Sci. **160**, 230 (1937).
[36] X. Gonze and C. Lee, Phys. Rev. B **55**, 10355 (1997).
[37] X. Gonze, Phys. Rev. B **55**, 10337 (1997).
[38] S. Baroni, P. Giannozzi, and A. Testa, Phys. Rev. Lett. **58**, 1861 (1987).
[39] F. Giustino, Rev. Mod. Phys. **89**, 015003 (2017).
[40] F. Mauri, O. Zakharov, S. de Gironcoli, S. G. Louie, and M. L. Cohen, Phys. Rev. Lett. **77**, 1151 (1996).
[41] J. Sjakste, N. Vast, and V. Tyuterev, Phys. Rev. Lett. **99**, 236405 (2007).
[42] M. Bernardi, Eur. Phys. J. B **89**, 239 (2016).
[43] M. Bernardi, D. Vigil-Fowler, J. Lischner, J. B. Neaton, and S. G. Louie, Phys. Rev. Lett. **112**, 257402 (2014).
[44] F. Giustino, J. R. Yates, I. Souza, M. L. Cohen, and S. G. Louie, Phys. Rev. Lett. **98**, 047005 (2007).
[45] J. Sjakste, N. Vast, M. Calandra, and F. Mauri, Phys. Rev. B **92**, 054307 (2015).
[46] C. Verdi and F. Giustino, Phys. Rev. Lett. **115**, 176401 (2015).
[47] R. T. Williams, Q. Li, J. Q. Grim, K. B. Ucer, G. A. Bizarri, and W. W. Moses, in *Hard X-Ray, Gamma-Ray, and Neutron Detector Physics XII*, Proc. SPIE 7805 (Society of Photo-Optical Instrumentation Engineers, Bellingham, WA, 2010), p. 78050K.
[48] F. Gao, Y. L. Xie, Z. G. Wang, S. Kerisit, D. X. Wu, L. W. Campbell, R. M. Van Ginhoven, and M. Prange, J. Appl. Phys. **114**, 173512 (2013).
[49] S. Baroni, S. de Gironcoli, A. D. Corso, and P. Giannozzi, Rev. Mod. Phys. **73**, 515 (2001).
[50] S. Kerisit, K. M. Rosso, B. D. Cannon, F. Gao, and Y. Xie, J. Appl. Phys. **105**, 114915 (2009).
[51] M. Prange, D. Wu, Y. Xie, L. W. Campbell, F. Gao, and S. Kerisit, *Hard X-Ray, Gamma-Ray, and Neutron Detector Physics XVI*, Proc. SPIE 9213 (Society of Photo-Optical Instrumentation Engineers, Bellingham, WA, 2014), p. 92130L.
[52] X. Gonze, B. Amadon, P.-M. Anglade, J.-M. Beuken, F. Bottin, P. Boulanger, F. Bruneval, D. Caliste, R. Caracas, M. Côté *et al.*, Comput. Phys. Commun. **180**, 2582 (2009).
[53] X. Gonze, J.-M. Beuken, R. Caracas, F. Detraux, M. Fuchs, G.-M. Rignanese, L. Sindic, M. Verstraete, G. Zerah, F. Jollet *et al.*, Comput. Mater. Sci. **25**, 478 (2002).
[54] P. Vogl, Phys. Rev. B **13**, 694 (1976).
[55] J. S. Melvin, J. D. Pirie, and T. Smith, Phys. Rev. **175**, 1082 (1968).
[56] A. D. B. Woods, W. Cochran, and B. N. Brockhouse, Phys. Rev. **119**, 980 (1960).
[57] S. Ganesan, E. Burstein, A. M. Karo, and J. R. Hardy, J. Phys. France **26**, 639 (1965).
[58] N. Troullier and J. L. Martins, Phys. Rev. B **43**, 1993 (1991).
[59] S. Goedecker, M. Teter, and J. Hutter, Phys. Rev. B **54**, 1703 (1996).
[60] J. P. Perdew, K. Burke, and M. Ernzerhof, Phys. Rev. Lett. **77**, 3865 (1996).
[61] M. Fuchs and M. Scheffler, Comput. Phys. Commun. **119**, 67 (1999).
[62] J. N. Bradford and S. Woolf, J. Appl. Phys. **70**, 490 (1991).
[63] L. H. Holway and D. W. Fradin, J. Appl. Phys. **46**, 279 (1975).
[64] M. V. Fischetti, D. J. DiMaria, S. D. Brorson, T. N. Theis, and J. R. Kirtley, Phys. Rev. B **31**, 8124 (1985).
[65] T. Boutboul, A. Akkerman, A. Gibrekhterman, A. Breskin, and R. Chechik, J. Appl. Phys. **86**, 5841 (1999).
[66] N. Ross, J. Zhao, and R. Angel, J. Solid State Chem. **177**, 1276 (2004).
[67] H. Bärnighausen and N. Schulz, Acta Crystallogr. Sect. **25**, 1104 (1969).
[68] S. Gražulis, D. Chateigner, R. T. Downs, A. F. T. Yokochi, M. Quirós, L. Lutterotti, E. Manakova, J. Butkus, P. Moeck, and A. Le Bail, J. Appl. Crystallogr. **42**, 726 (2009).